Phys Chem Minerals (2013) 40:647–657
DOI 10.1007/s00269-013-0600-x

ORIGINAL PAPER

# Phase relations in the carbon-saturated C–Mg–Fe–Si–O system and C and Si solubility in liquid Fe at high pressure and temperature: implications for planetary interiors

**Suguru Takahashi · Eiji Ohtani · Hidenori Terasaki · Yoshinori Ito · Yuki Shibazaki · Miho Ishii · Ken-ichi Funakoshi · Yuji Higo**

Received: 11 October 2012 / Accepted: 5 May 2013 / Published online: 18 May 2013


**Abstract** The phase and melting relations of the C-saturated C–Mg–Fe–Si–O system were investigated at high pressure and temperature to understand the role of carbon in the structure of the Earth, terrestrial planets, and carbon-enriched extraterrestrial planets. The phase relations were studied using two types of experiments at 4 GPa: analyses of recovered samples and in situ X-ray diffractions. Our experiments revealed that the composition of metallic iron melts changes from a C-rich composition with up to about 5 wt.% C under oxidizing conditions ($\Delta IW = -1.7$ to $-1.2$, where $\Delta IW$ is the deviation of the oxygen fugacity ($fO_2$) from an iron-wüstite (IW) buffer) to a C-depleted composition with 21 wt.% Si under reducing conditions ($\Delta IW < -3.3$) at 4 GPa and 1,873 K. SiC grains also coexisted with the Fe–Si melt under the most reducing conditions. The solubility of C in liquid Fe increased with increasing $fO_2$, whereas the solubility of Si decreased with increasing $fO_2$. The carbon-bearing phases were graphite, $Fe_3C$, SiC, and Fe alloy melt (Fe–C or Fe–Si–C melts) under the redox conditions applied at 4 GPa, but carbonate was not observed under our experimental conditions. The phase relations observed in this study can be applicable to the Earth and other planets. In hypothetical reducing carbon planets ($\Delta IW < -6.2$), graphite/diamond and/or SiC exist in the mantle, whereas the core would be an Fe–Si alloy containing very small amount of C even in the carbon-enriched planets. The mutually exclusive nature of C and Si may be important also for considering the light elements of the Earth's core.

**Keywords** Carbon-enriched planet · Oxygen fugacity · Solubility · Core composition · Deep carbon cycle

S. Takahashi (✉) · E. Ohtani · H. Terasaki · Y. Ito · Y. Shibazaki · M. Ishii
Department of Earth and Planetary Material Sciences, Tohoku University, 6-3 Aoba, Aramaki, Aoba-ku, Sendai 980-8571, Japan
e-mail: stakahashi@s.tohoku.ac.jp

H. Terasaki
Department of Earth and Space Science, Osaka University, 1-1 Machikaneyama-cho, Toyonaka 560-0043, Japan

Y. Shibazaki
Geophysical Laboratory, Carnegie Institution of Washington, 5251 Broad Branch Road, NW, Washington, DC 20015, USA

K. Funakoshi · Y. Higo
Japan Synchrotron Radiation Research Institute, 1-1-1 Kouto, Sayo 679-5198, Japan

## Introduction

Knowledge of carbon abundance in the Earth is very important for understanding the planet's carbon budget, including $CO_2$ in the atmosphere and oceans. Furthermore, the abundance and the forms of carbon in carbonaceous chondrites (Keil 1968) and ureilites (Zolensky et al. 2010) are essential to the understanding of how carbon can be taken into a planetary body in its formation process. The abundance of carbon in some of the stars with exoplanets, such as the circumstellar gas around Beta Pictoris, has been estimated to be 100 times higher than that in CI chondrites (e.g., Roberge et al. 2006; Lagrange et al. 2009). Wood and Hashimoto (1993) reported that condensates in the nebula with the ratio of carbon to oxygen (C/O) in the nebula is greater than unity are very different from those with C/O below unity. In particular, carbides, such as $Fe_3C$ and SiC, are reported to be stable phases in nebulae with C/O greater than unity, and the carbon-enriched planets ("carbon planet") may be formed in such nebula (Seager et al. 2007).

The interior of carbon planets is expected to be composed of carbon compounds, such as carbides ($Fe_3C$ and SiC), carbonates ($MgCO_3$ and $FeCO_3$), graphite, and diamond, although carbon planets have not yet been observed directly.

It has been argued by many authors that, in the case of the Earth, the subduction of altered (carbonated) oceanic crust together with marine sediments provides a large flux of carbonates into the mantle (Molina and Poli 2000; Kerrick and Connolly 2001; Dasgupta et al. 2004; Dasgupta and Hirschmann 2010; Kiseeva et al. 2012). Magnesite ($MgCO_3$) is stable up to the pressure and temperature conditions of the D″ layer; therefore, carbon is likely to be transported to the core–mantle boundary (Isshiki et al. 2004). On the other hand, if metallic iron is saturated in the lower mantle because of a disproportionate reaction of perovskite (Frost et al. 2004), carbon may be stored in Fe alloy and/or Fe-carbide (Dasgupta and Hirschmann 2010). Furthermore, it has been proposed that carbon is one of the candidates for the light elements needed to explain the Earth's core density deficit (e.g., Wood 1993; Dasgupta et al. 2013).

Although there are many studies on carbon–iron and carbon–silicate systems, experimental studies on the phase relations in the system of carbon–silicate (or oxides)–iron are still very limited (Siebert et al. 2005; Dasgupta et al. 2013) despite their importance in meteorite parent bodies and planetary interiors. In this study, we performed high-pressure experiments, based on chemical analyses of recovered samples and in situ X-ray diffraction experiments at 4 GPa, to investigate the phase relations in a carbon-saturated C–Mg–Fe–Si–O system. Our results are applied to the behavior of carbon in the interiors of terrestrial planets and hypothetical carbon planets.

## Experimental procedure

We performed experiments with several different starting compositions using two types of capsule (MgO or graphite), as described below. MgO capsules were used in experiments to determine the influence of metal composition and oxygen fugacity ($fO_2$). However, MgO capsules react with Si and $SiO_2$ in the sample to form olivine (Gessmann et al. 2001). Graphite capsules were also used to avoid a reaction of the capsule with Si or $SiO_2$ and to determine the stable oxide/silicate phases. The phase relations were determined based on textural observations and chemical analyses of the recovered samples from quench experiments, as well as on in situ X-ray diffraction experiments at high pressure and temperatures.

The starting materials were powdered mixtures of several different ratios of oxides (MgO: periclase; $SiO_2$: quartz), silicates ($(Mg_{1.8}, Fe_{0.2})SiO_4$: San Carlos olivine), carbonate ($MgCO_3$: magnesite), iron (Fe), silicon (Si), and graphite (C). Fe and Si were mixed in the form of the oxides or elemental metals to produce a wide $fO_2$ range. The compositions and mixed phases of the starting materials used are summarized in Table 1. The starting materials used the reagents with mixing ratios of Mg:Fe:Si:O:C = 1:1:1:x:3, with various values of the oxygen content, x. The C/O ratio was always set to be in the range from 0.94 to 3.0; this is greater than the ratio in CI chondrites, which is 0.48 (Anders and Grevesse 1989).

Quenching experiments were carried out using a 3,000-ton Kawai-type multi-anvil apparatus installed at Tohoku University, Japan. Tungsten carbide cubes of 26 mm length with 12 mm truncated edges were used as the second-stage anvils. Two capsules were placed in a cylindrical graphite heater. The temperature was measured using a W3%Re–W25%Re thermocouple whose junction was located near the capsule inside the heater. All the quench experiments were performed at 4 GPa and 1,873 K for 5 h. The details of the cell assembly and experiments are described elsewhere (Hayashi et al. 2009). Recovered samples were mounted in epoxy resin and polished for chemical analyses.

Chemical analyses of the recovered samples from the quench experiments were performed using a wavelength-dispersive electron microprobe (JEOL, JXA-8800) installed at Tohoku University. Elemental standards used for the analyses of the silicate phases in the recovered samples were forsterite ($Mg_2SiO_4$) for Si and Mg and fayalite ($Fe_2SiO_4$) for Fe. For the metallic phases in the recovered samples, the standards were pure iron for Fe, pure silicon for Si, synthesized $Fe_3C$ for C, and hematite ($Fe_2O_3$) for O. The samples and standards were first coated with carbon to analyze the silicate/oxide phases. An accelerating voltage and a beam current were applied at 15 kV and 15 nA, respectively. After the analyses of the silicate/oxide phases, the carbon coating layer was removed and the samples and standards were coated with Al to analyze the metallic phases. An accelerating voltage of 15 kV and a beam current of 90 nA were used to analyze the metallic phases, and the LDE1H crystal of the electron microprobe was used to measure the carbon content in the metallic phases. For quantitative analyses of heterogeneous quenched metallic liquid, we used a defocused beam ($\sim$10 μm). Less than 0.1 wt.% of carbon was detected in the pure iron standard. This presence was derived from carbon contamination from the epoxy resin, vacuum greases, or the residual oil vapors of the diffusion of pump oil in the microprobe chamber. No corrections were made for this contribution, and the present detection limit for C in the metallic phases was defined as 0.1 wt.%. The data obtained were corrected using the ZAF routine.

**Table 1** Compositions of the starting materials (in wt.%)

| Run no.[a] | T1859A M882A | T1859B M882B | T1860A M884A | T1860B T1879 M884B | T1862 |
|---|---|---|---|---|---|
| Starting mixture | Olivine[b], quartz, iron, graphite | Olivine, silicon, iron, graphite | Periclase, quartz, iron, graphite | Periclase, silicon, iron, graphite | Magnesite, silicon, iron, graphite |
| Mg | 12.5 | 13.5 | 12.6 | 15.2 | 12.6 |
| Fe | 28.7 | 31.1 | 29.0 | 34.8 | 29.0 |
| Si | 14.5 | 15.6 | 14.6 | 17.5 | 14.6 |
| O | 25.7 | 19.8 | 25.0 | 10.0 | 25.0 |
| C | 18.5 | 20.0 | 18.7 | 22.5 | 18.7 |
| Total | 100.0 | 100.0 | 100.0 | 100.0 | 100.0 |
| C/O[c] | 0.96 | 1.35 | 1.00 | 3.00 | 1.00 |

[a] T1859A, T1859B, T1860A, T1860B, T1862, and T1879 are quench experiments and M882A, M882B, M884A, and M884B are in situ X-ray diffraction experiments

[b] The olivine used was San Carlos olivine

[c] The atomic ratios of carbon to oxygen in the starting compositions

The oxygen fugacity of the sample was determined based on the reaction between Fe in the sample and the MgO capsule. We calculated $fO_2$ assuming a non-ideal solution in both silicate and metallic melt (e.g., Wade et al. 2012). A value of $\log fO_2$ ($\Delta$IW), which corresponds to the deviation of the oxygen fugacity from an iron-wüstite (IW) buffer on a logarithmic scale, was estimated using the following equation:

$$\log fO_2(\Delta\mathrm{IW}) = 2\log\frac{a_{\mathrm{FeO}}^{\mathrm{Mw}}}{a_{\mathrm{Fe}}^{\mathrm{met}}} = 2\log\frac{\gamma_{\mathrm{FeO}}^{\mathrm{Mw}}\cdot X_{\mathrm{FeO}}^{\mathrm{Mw}}}{\gamma_{\mathrm{Fe}}^{\mathrm{met}}\cdot X_{\mathrm{Fe}}^{\mathrm{met}}}, \quad (1)$$

where $a_{\mathrm{Fe}}^{\mathrm{met}}$, $\gamma_{\mathrm{Fe}}^{\mathrm{met}}$, and $X_{\mathrm{Fe}}^{\mathrm{met}}$ are the activity, activity coefficient, and mole fraction of Fe in the metallic phase of the recovered sample and $a_{\mathrm{FeO}}^{\mathrm{Mw}}$, $\gamma_{\mathrm{FeO}}^{\mathrm{Mw}}$, and $X_{\mathrm{FeO}}^{\mathrm{Mw}}$ are the activity, activity coefficient, and mole fraction of FeO in the MgO capsule in contact with the metal in the sample. $\gamma_{\mathrm{Fe}}^{\mathrm{met}}$ was determined by the modified ε-model (Wagner 1952; Ma 2001; Wade et al. 2012). $\gamma_{\mathrm{FeO}}^{\mathrm{Mw}}$ was determined using the equation by Frost et al. (2010). In Run T1879, in which MgO was not observed in the run product using a graphite capsule, the value of $\Delta$IW was estimated from the value of $X_{\mathrm{FeO}}$ of magnesiowüstite calculated from that of olivine based on the exchange partition coefficient $K^{\mathrm{Ol/Mw}}$, which was defined as:

$$K^{\mathrm{Ol/Mw}} = \frac{X_{\mathrm{FeO}}^{\mathrm{Ol}}/X_{\mathrm{MgO}}^{\mathrm{Ol}}}{X_{\mathrm{FeO}}^{\mathrm{Mw}}/X_{\mathrm{MgO}}^{\mathrm{Mw}}}, \quad (2)$$

where $X_{\mathrm{M}}^{\mathrm{N}}$ is the mole fraction of component "M" (MgO or FeO) in phase "N" (olivine or magnesiowüstite) (Fei et al. 1991). The value of $K^{\mathrm{Ol/Mw}}$ in Run T1879 was estimated from runs in which magnesiowüstite was observed in the run product, and it was found to be $0.62 \pm 0.04$.

We performed in situ X-ray diffraction experiments to determine the assemblage of stable silicates and metallic phases at high pressure and temperature. These experiments were carried out using a 1,500-ton Kawai-type multi-anvil apparatus ("SPEED-Mk.II") installed at the BL04B1 beamline at the SPring-8 synchrotron radiation facility in Japan. An energy-dispersive X-ray diffraction method was used. A Ge solid-state detector connected to a multichannel analyzer was used to acquire the X-ray data. The energy–channel relationship of the multichannel analyzer was calibrated using the characteristic X-rays of Cu, La, Mo, Ag, Ta, Pt, Au, and Pb. The diffraction angle was fixed to $2\theta = 5.5°$. The incident X-ray beam was collimated to a narrow beam with dimensions of 0.1 mm in the horizontal direction and 0.2 mm in the vertical direction. The experiments were performed at 4 GPa up to 1,873 K. The diffraction patterns of the samples were collected for 200–300 s for each 100–300 K temperature interval between 300 and 1,873 K. It took 5–6 h to increase the temperature up to 1,873 K. The cell assembly used in the experiments was basically the same as that used in the quench experiments. The sample was contained in a graphite capsule. MgO was used in the central part of the pressure medium for the X-ray path. The experimental pressure was determined using the equation of state of hexagonal boron nitride by measuring the lattice parameters (Urakawa et al. 1993). Diffraction patterns were analyzed using the "X-ray Ana" software programmed by H. Kaneko and the "PD Indexer" software programmed by Y. Seto.

## Results

### Textural observations and chemical analyses of the recovered samples

The observed phases and $\Delta$IW values calculated from $X_{\mathrm{FeO}}$ and $X_{\mathrm{Fe}}$ in Eq. (1) for each starting material are summarized in Table 2. The values of $\Delta$IW ranged from $-6.19$ to $-1.18$. The dendritic textures of the metallic phases

indicated that the phases melted below 1873 K at 4 GPa. Backscattered electron images of the recovered samples from the most oxidizing and reducing conditions are shown in Figs. 1 and 2, respectively. We analyzed the compositions of quenched liquid Fe in the area C in Figs. 1a and 2a. We used a defocused beam, whose diameter was 5–10 μm to analyze the bulk compositions of quenched liquid Fe. In addition, we analyzed several quenched Fe grains with a smaller grain size (>1 μm) in the area B using a defocused beam of 1–5 μm. There was no significant difference in composition between the quenched metallic liquids in the area B and C. We showed the results of analyses including those from the area B and C in Table 2 The compositions of liquid Fe varied with the oxygen fugacity conditions, as described below. In the case of the experiments using the MgO capsule, only olivine was observed as a silicate phase. By contrast, in the case of the experiments using a graphite capsule, a few tiny SiC grains were observed at the edge of the olivine grains. In the samples recovered from relatively oxidizing conditions ($\Delta IW = -1.71$ to $-1.18$, Runs T1859A, T1860A, and T1862), the observed liquid Fe alloy phases contained a large amount of C, 4.1–5.2 wt.% without dissolving of Si, whereas in the samples recovered from relatively reducing conditions ($\Delta IW = -3.33$ to $-2.31$, Runs T1859B and T1860B), the observed liquid Fe alloy was an Fe–Si–C composition (Si = 20.97–9.89 wt.%, C = 0.5–2.0 wt.%). In the sample subjected to the most reducing conditions ($\Delta IW = -6.19$, Run T1879), the observed liquid Fe alloy phase contained a large amount of Si (up to 19.38 wt.%) without dissolving of C. A graphite phase was observed in all the recovered samples, whereas carbonates (such as magnesite, $MgCO_3$, and siderite, $FeCO_3$) were not observed. They were not observed even in the sample subjected to the most oxidizing conditions in this study ($\Delta IW = -1.18$), in which $MgCO_3$ was present in the starting material (Run T1862).

The value of Fe# (=100 × FeO/(MgO + FeO)) of olivine changed from 5.58 to 0.70 with decreasing ΔIW from −1.18 to −2.31, as shown in Table 2. Under further reducing conditions, $\Delta IW < -2.31$, there was little change in the value of Fe#, 0.70–0.96. The Fe# of olivine was lower than that of San Carlos olivine (Fe# = 10) in Runs T1859A and T1859B, in which San Carlos olivine was used as a starting material. It seems that the FeO in olivine was reduced to Fe during the experiment.

## X-ray diffraction patterns

We confirmed the stable phases of the silicates and Fe alloy before melting and determined the melting temperature of the Fe alloy based on the in situ X-ray diffraction. The diffraction results for different starting materials are listed in Table 3. Figure 3a, b shows typical examples of the X-ray diffraction patterns obtained at 4 GPa and at high temperatures for the oxidizing starting assemblage M882A (olivine + iron + quartz + graphite) and the most reducing starting assemblage M884B (periclase + iron + silicon + graphite), respectively. The observed phases are summarized in Table 3. In Run M882A, the diffraction peaks from $Fe_3C$ and orthopyroxene appeared at 1,073 and 1,373 K, respectively. The $Fe_3C$ peaks suddenly disappeared at 1,673 K, and a halo pattern appeared around the position where the intense $Fe_3C$ peaks were observed, suggesting that $Fe_3C$ was molten at this temperature. The melting temperature of $Fe_3C$ would then be lower than that reported by Lord et al. (2009), but is consistent with the result of Nakajima et al. (2009). Olivine, orthopyroxene, and graphite coexisted stably together with the liquid iron phase above 1,673 K.

In the most reducing starting assemblage (Run M884B), diffraction peaks attributed to $Fe_3C$ appeared at 1,073 K. The $Fe_3C$ peaks disappeared, and peaks ascribed to εFeSi (Wood et al. 1996) and βSiC appeared at 1,373 K. βSiC has a cubic zinc-blende structure under the present experimental conditions, which is consistent with the results of Van Vechten (1973). At 1,673 K, the peaks from εFeSi disappeared and a halo pattern appeared, suggesting that the εFeSi phase had melted. This indicates that the εFeSi and βSiC phases are stable at high temperatures above 1,373 K at 4 GPa under reducing conditions, whereas $Fe_3C$ is stable under oxidizing conditions. This result is consistent with the composition of the liquid iron in the quench experiments as described above. Olivine and orthopyroxene are stable as silicate phases above 1,373 K under the oxidizing conditions, and magnesiowüstite is stable under the most reducing condition. Graphite was stable under all the experimental conditions.

Compared with the results of the quench experiments, apparent differences were recognized in the silicate phases. The results based on in situ X-ray diffraction experiments using graphite capsules revealed that the stable oxide and silicate phases were magnesiowüstite in the relatively reducing conditions, and olivine and pyroxene in the relatively oxidizing conditions at 4 GPa. By contrast, olivine was the only silicate phase observed in quench experiments, in which MgO capsules were used (Table 2). The fact that olivine was found adjacent to the MgO capsule indicates that additional olivine was formed as a result of a reaction between the Si or $SiO_2$ in the sample and the MgO capsule. In the case of metallic phases, observed phases in the in situ X-ray experiments were consistent with those in the quench experiments, that is, Fe–Si alloy was formed at high temperature and melted under the reducing conditions, whereas $Fe_3C$ was observed under the oxidizing conditions.

**Table 2** Summary of the quench experiments: phase assemblages of the starting materials, sample capsule, compositions of the phases in the run products recovered from the quench experiments, and the oxygen fugacity conditions (see main text)

| Run no. | T1859A | T1859B | T1860A | T1860B | T1862 | T1879 |
|---|---|---|---|---|---|---|
| C/O | 0.96 | 1.35 | 1.00 | 3.00 | 1.00 | 3.00 |
| Capsule | MgO | MgO | MgO | MgO | MgO | Graphite |
| Starting composition | Olivine, Fe, $SiO_2$, graphite | Olivine, Fe, Si, graphite | MgO, Fe, $SiO_2$, graphite | MgO, Fe, Si, graphite | $MgCO_3$, Fe, Si, graphite | MgO, Fe, Si, graphite |
| Observed phases | Liquid iron, olivine, graphite | Liquid iron, olivine, graphite | Liquid iron, olivine, graphite | Liquid iron, olivine, graphite | Liquid iron, olivine, graphite | Liquid iron, olivine, graphite, SiC |
| Liquid iron (wt.%) | | | | | | |
| Fe | 93.09 (0.52)[a] | 88.18 (0.23) | 92.23 (0.41) | 77.85 (0.74) | 94.57 (0.32) | 80.62 (0.48) |
| Si | – | 9.89 (0.41) | – | 20.97 (0.66) | – | 19.38 (0.27) |
| C | 4.1 (0.3) | 2.0 (0.2) | 4.7 (0.3) | 0.5 (0.5) | 5.2 (0.2) | – |
| O | 0.24 (0.03) | 0.22 (0.03) | 0.24 (0.02) | 0.25 (0.03) | 0.20 (0.03) | 0.39 (0.08) |
| Total | 97.4 | 100.3 | 97.1 | 99.6 | 100.0 | 100.83 |
| $n$[b] | 11 | 11 | 11 | 10 | 11 | 8 |
| Olivine (wt.%) | | | | | | |
| $SiO_2$ | 41.79 (0.46) | 42.07 (0.76) | 42.28 (0.34) | 42.93 (0.45) | 41.15 (0.57) | 43.26 (0.68) |
| MgO | 53.60 (0.85) | 56.70 (0.50) | 53.85 (0.30) | 55.98 (0.54) | 52.21 (0.87) | 56.65 (0.93) |
| FeO | 2.91 (0.45) | 0.71 (0.33) | 3.25 (0.36) | 0.97 (0.22) | 5.50 (0.89) | 0.76 (0.36) |
| Total | 98.30 | 99.49 | 99.38 | 99.89 | 98.87 | 100.67 |
| $n$[b] | 5 | 4 | 7 | 5 | 5 | 5 |
| Fe# | 2.96 (0.49) | 0.70 (0.32) | 3.28 (0.38) | 0.96 (0.22) | 5.58 (0.99) | 0.74 (0.35) |
| SiC (wt.%) | | | | | | |
| Fe | – | – | – | – | – | 2.11 (0.53) |
| Si | – | – | – | – | – | 56.03 (2.82) |
| C | – | – | – | – | – | 43.46 (3.23) |
| Total | – | – | – | – | – | 101.61 |
| $n$[b] | – | – | – | – | – | 2 |
| Magnesiowüstite (wt.%) | | | | | | |
| $SiO_2$ | 0.01 (0.01) | 0.03 (0.06) | 0.01 (0.03) | 0.06 (0.04) | 0.02 (0.01) | – |
| MgO | 90.17 (1.65) | 97.85 (0.63) | 90.11 (3.40) | 97.40 (0.80) | 85.94 (4.00) | – |
| FeO | 8.38 (1.19) | 0.31 (0.07) | 8.91 (3.82) | 0.42 (0.11) | 13.91 (4.46) | – |
| Total | 98.56 | 98.19 | 99.04 | 97.87 | 99.86 | – |
| $n$[b] | 7 | 5 | 5 | 3 | 5 | – |
| ΔIW | −1.71 (0.14) | −2.31 (0.21) | −1.59 (0.39) | −3.33 (0.26) | −1.18 (0.29) | −6.19 (0.47) |

All the experiments were conducted at 4 GPa and 1,873 K

[a] The numbers in parenthesis denote the standard deviation

[b] The number of analytical points

## Discussion

### The influence of $fO_2$ and Si on the solubility of C in liquid Fe

The present results indicate an inverse correlation between the solubilities of C and Si in liquid Fe (Fig. 4a). The inset of Fig. 4a shows the amount of C and Si in liquid Fe as a function of ΔIW. This figure shows that the solubility of Si in liquid Fe increases with decreasing oxygen fugacity. The partition coefficient ($D$) of Si between metallic and silicate melts is expressed as follows:

$$\log D^{\text{metal}}_{\text{silicate}}(\text{Si}) = \left[\frac{X^{\text{metal}}_{\text{Si}}}{X^{\text{silicate}}_{\text{SiO}_2}}\right], \quad (3)$$

where $D$ is the partition coefficient for Si and $X^{\text{N}}_{\text{M}}$ is the mole fraction of component "M" (Si or $SiO_2$) in phase "N" (metal or silicate). The relationship between the partition coefficient and the oxygen fugacity can be

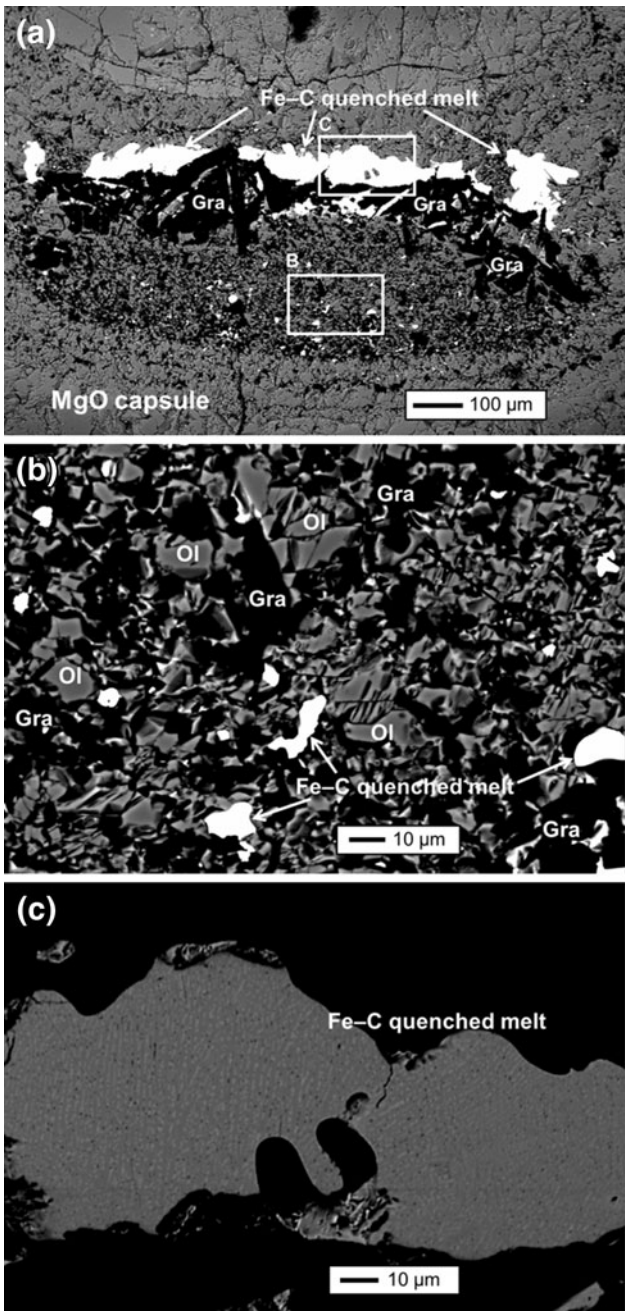


**Fig. 1** Backscattered electron images of the recovered sample T1862 (starting composition = $MgCO_3$ + Fe + Si + graphite) at 4 GPa and 1,873 K and ΔIW = −1.18. **a** The entire sample. **b** High-magnification image of the area B in (**a**); olivine (Ol), graphite (Gra), and Fe–C quenched melt are observed. **c** Close-up image of the area C in (**a**); a dendritic texture is observed in Fe–C quenched melt

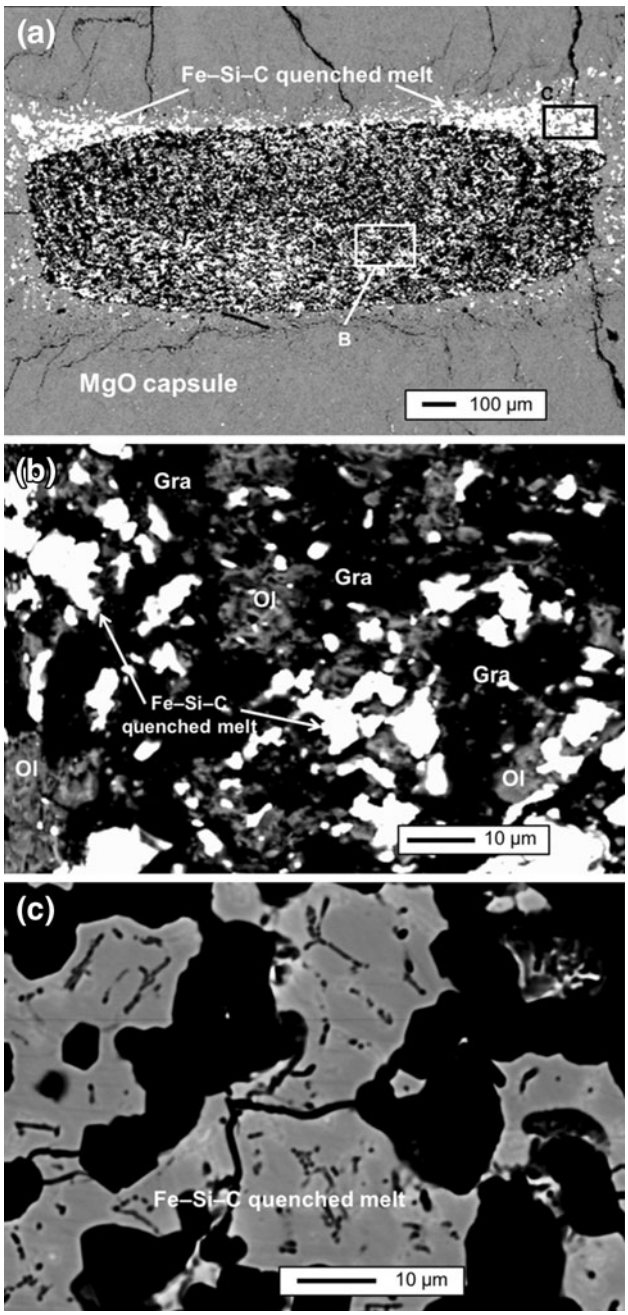


**Fig. 2** Backscattered electron images of the recovered sample T1860B (starting composition = MgO + Fe + Si + graphite) at 4 GPa and 1,873 K and ΔIW = −3.33. **a** The entire sample. **b** High-magnification image of the area B in (**a**); olivine (Ol), graphite (Gra), and Fe–Si–C quenched melt are observed. **c** Close-up image of the area C in (**a**); a dendritic texture is observed in Fe–Si–C quenched melt

expressed as follows (e.g., Corgne et al. 2008a; Mann et al. 2009):

$$\log D^{\text{metal}}_{\text{silicate}}(\text{Si}) = -\Delta\text{IW} + \text{const.} \quad (4)$$

The equation indicates that $D^{\text{metal}}_{\text{silicate}}(\text{Si})$ increases with decreasing ΔIW, leading to an increase in $X^{\text{metal}}_{\text{Si}}$. This tendency is consistent with the present experimental results (Fig. 4a, inset). On the other hand, the amount of C in liquid Fe increased with increasing ΔIW. The tendency observed in this study is consistent with that at 1 atm at 1,873 K (Chipman et al. 1954) and at 1,813 K (Ohtani 1955), as shown in Fig. 4a. Thus, the C solubility depends

**Table 3** Changes in observed phase assemblages in the in situ X-ray diffraction experiments at 4 GPa with increasing temperature

| Run no. | 300 K | 1,073 K | 1,373 K | 1,673 K | 1,873 K |
|---|---|---|---|---|---|
| M882A | Ol, αFe, Qz[a], Gra | Ol, $Fe_3C$, Coe, Gra | Ol, Px, $Fe_3C$, Gra | Ol, Px, Gra, liquid | Ol, Px, Gra, liquid |
| M882B | Ol, αFe, Si, Gra | Ol, $Fe_3C$, Si, Gra | Ol, Px, $Fe_3C$, Gra | Ol, Px, Gra, liquid | Ol, Px, Gra, liquid |
| M884A | MgO, αFe, Qz, Gra | Ol, MgO, $Fe_3C$, Coe, Gra | Ol, Px, $Fe_3C$, Gra | Ol, Px, Gra, liquid | Ol, Px, Gra, liquid |
| M884B | MgO, αFe, Si, Gra | MgO, $Fe_3C$, Si, Gra | MgO, εFeSi, βSiC, Gra | MgO, βSiC, Gra, liquid | MgO, βSiC, Gra, liquid |

*Gra* graphite, *Ol* olivine, *Px* pyroxene, *Qz* quartz, *Coe* coesite, *MgO* periclase, *αFe* bcc-iron, *Si* diamond cubic structure silicon, $Fe_3C$ cementite, *εFeSi* B20 structured FeSi, and *βSiC* cubic zinc-blende structure silicon carbide

[a] Quartz was assumed to be a metastable phase at 4 GPa and 1,073 K

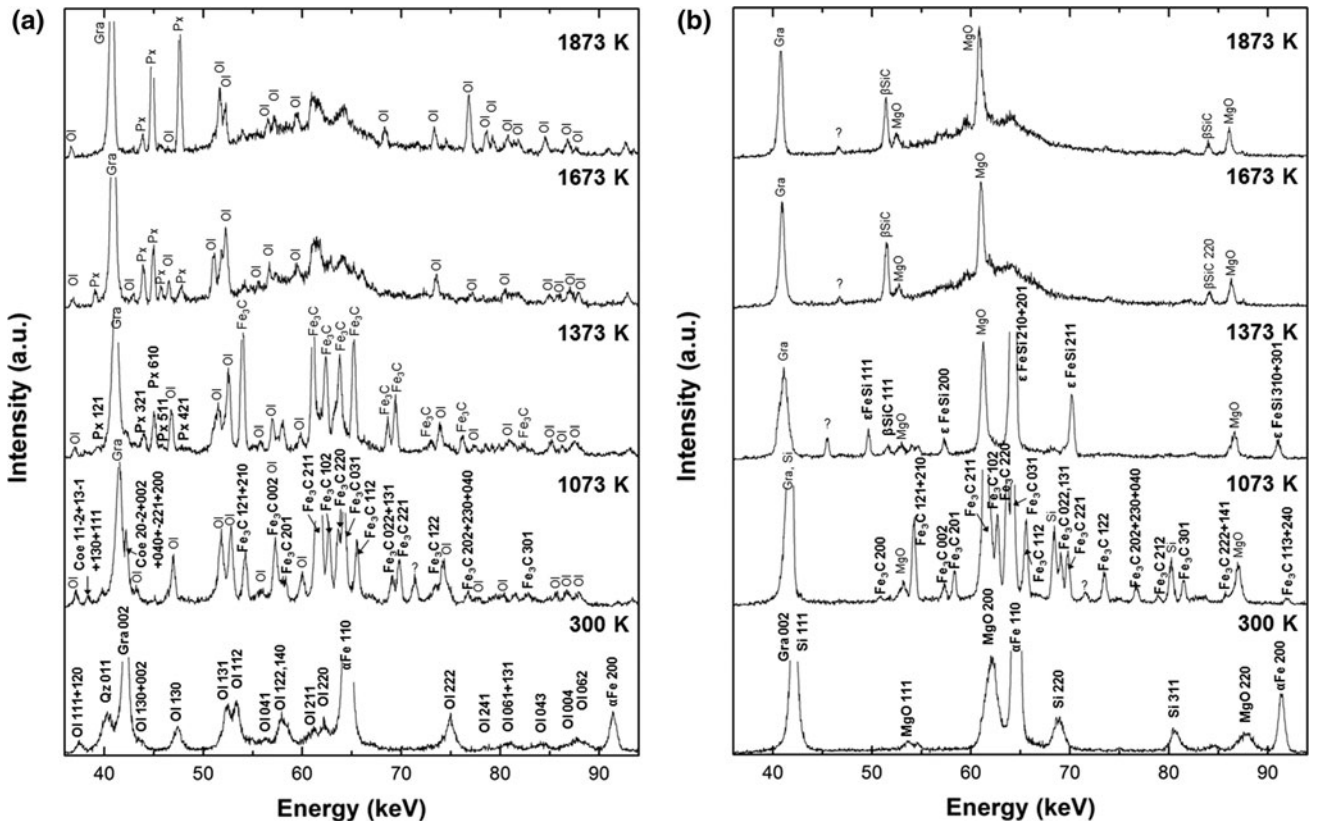


**Fig. 3** In situ X-ray diffraction patterns of the runs conducted at 4 GPa and 300, 1,073, 1,373, 1,673, and 1,873 K using a mixture of **a** olivine, quartz, iron, and graphite as the starting material (M882A), and **b** periclase, silicon, iron, and graphite as the starting material (M884B). Abbreviations: *Gra* graphite, *Ol* olivine, *Px* pyroxene, *Qz* quartz, *Coe* coesite, *MgO* periclase, *αFe* bcc-iron, *Si* diamond cubic structure silicon, $Fe_3C$ cementite, *εFeSi* B20 structured FeSi, *βSiC* cubic zinc-blende structure silicon carbide

on the Si content in the metal and apparently also on $fO_2$ in the present Fe–C–Si–O system.

We compared the effect of light elements with the solubility of C, as shown in Fig. 4b. As shown in this figure, Si reduces the C solubility in liquid Fe more effectively than sulfur. In their studies of the Fe–C–S system, Corgne et al. (2008b) and Dasgupta et al. (2009) reported immiscibility between the C-rich molten Fe alloy and S-rich molten Fe alloy up to around 6 GPa. However, such immiscibility was not observed in the present Fe–Si–C system.

The C solubility in liquid Fe found in this study is plotted as a function of temperature and pressure together with the previous results in Fig. 5a, b. Although Siebert et al. (2011) calculated that C solubility has pressure dependence, the largest C solubility in this study at 4 GPa was identical to the values at 1 atm (Chipman 1972) and at 2 GPa (Dasgupta and Walker 2008). However, the C solubility at 5 GPa reported by Nakajima et al. (2009) is greater than that of other studies including ours (Fig. 5a). This difference in the C solubility between the results of

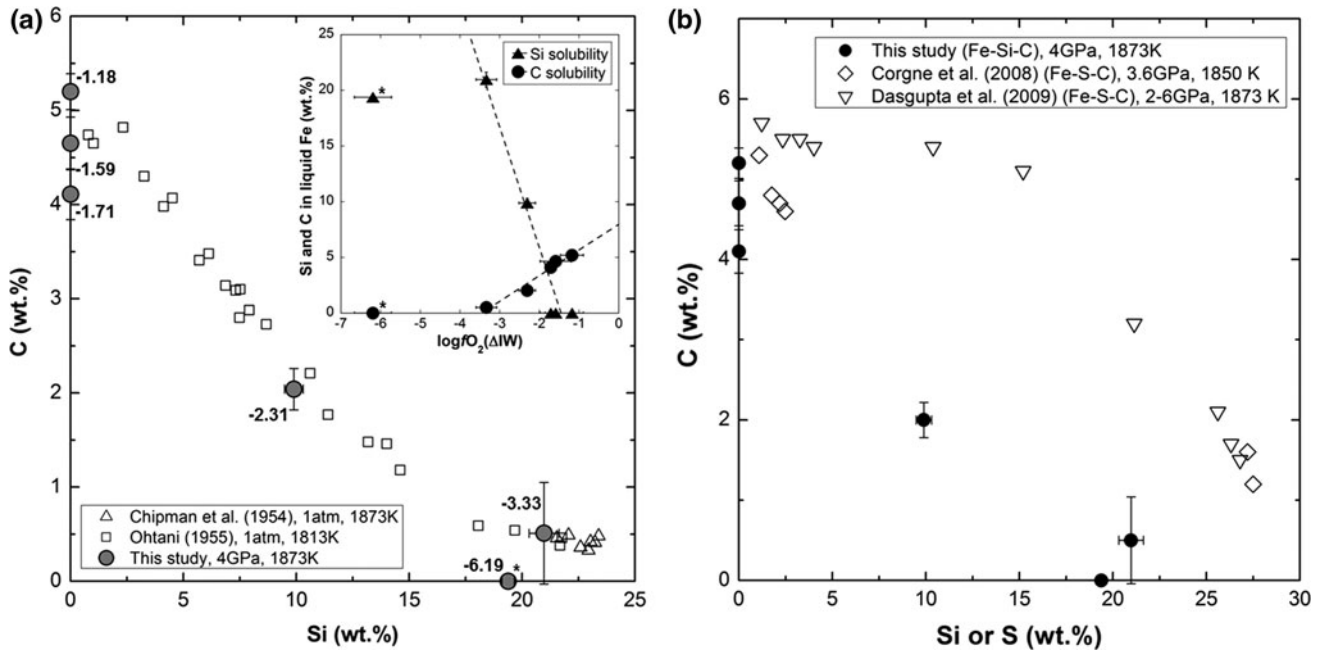


**Fig. 4** **a** The solubility of C in liquid Fe is plotted against the solubility of Si in liquid Fe. *Open triangles* show the solubilities of C and Si at 1 atm and 1,873 K reported by Chipman et al. (1954). *Open squares* indicate the solubilities of C and Si at 1 atm and 1,813 K reported by Ohtani (1955). *Gray circles* denote the present results at 4 GPa and 1,873 K. The *numbers* represent the oxygen fugacity conditions relative to the IW buffer (ΔIW) in this study. *Inset*: The contents of C and Si in liquid Fe as a function of the oxygen fugacity (ΔIW) at 4 GPa and 1,873 K. *Circles* and *triangles* show the C and Si contents, respectively. *A graphite capsule was used in this experiment. SiC is observed to coexist with quenched liquid Fe alloy in the recovered sample. **b** Comparison with the C solubility in liquid Fe in the Fe–Si–C system and the Fe–S–C system. *Open diamonds* and *inverted triangles* are the solubilities of C and S reported by Corgne et al. (2008b) and Dasgupta et al. (2009), respectively. *Solid circles* show the solubilities of C and Si in this study. We observed that Si reduces the C solubility in liquid Fe more effectively than S

Nakajima et al. (2009) and the others could be explained as follows. Nakajima et al. (2009) reported that the C solubility was measured including any graphite crystals coexisting with liquid Fe in the quenched samples. If not all of the graphite crystals in the quenched samples are the quench crystals formed from melt during quenching, then the C solubility is clearly overestimated. On the other hand, Dasgupta and Walker (2008) did not include the graphite crystals coexisting with liquid Fe and we did not observe these crystals in recovered samples. When graphite crystals coexisting with liquid Fe are removed from the measurement, the C solubility (=5.7 wt.% C in liquid Fe at 5 GPa and 1,873 K) is similar to the results of Chipman (1972), Wood (1993), Dasgupta and Walker (2008), and that under the most oxidizing condition in this study. The C solubility might be in the range of 5–6 wt.% under 1 atm–5 GPa at 1,873 K (Fig. 5b). We also plotted the recent results by Dasgupta et al. (2013) in Fig. 5a, b. They reported that the C solubility increased up to 6.83 wt.% when 4.80 wt.% Ni is contained in the liquid metal phase. Therefore, Fig. 5a, b suggests that the effects of pressure and temperature on the C solubility are very weak, although the C solubility strongly depends on the Ni solubility and the oxygen fugacity.

## Predictions regarding the interior of carbon planets

The present results may be applicable to the interiors of carbon planets and the parent bodies of ureilites with different C/O ratios and $fO_2$ conditions. We propose modeled interiors of a carbon-enriched extraterrestrial planet under each of relatively oxidizing and reducing conditions. The crust and mantle are considered to be composed of graphite/diamond and silicate minerals, and the composition of the core is likely to be either Fe–C or Fe–Si–C alloys under the $fO_2$ conditions of $\Delta IW = -3.33$ to $-1.18$. Conversely, in more reducing hypothetical planets ($\Delta IW < -6.19$), the mantle is possibly composed of graphite/diamond, SiC, and MgO, whereas the core would be an Fe–Si alloy containing a very small amount of C. It is noted that the core would contain a very small amount of carbon under these extremely reducing conditions, even in the carbon-enriched planets. In this argument, we ignored the phase changes associated with pressure. Because the internal pressure of the hypothetical carbon planets could be extremely high, the present results would be applicable only to the crust and uppermost mantle of the planets or to the core-formation process if this occurred at relatively shallow levels. Experimental studies at higher pressures are

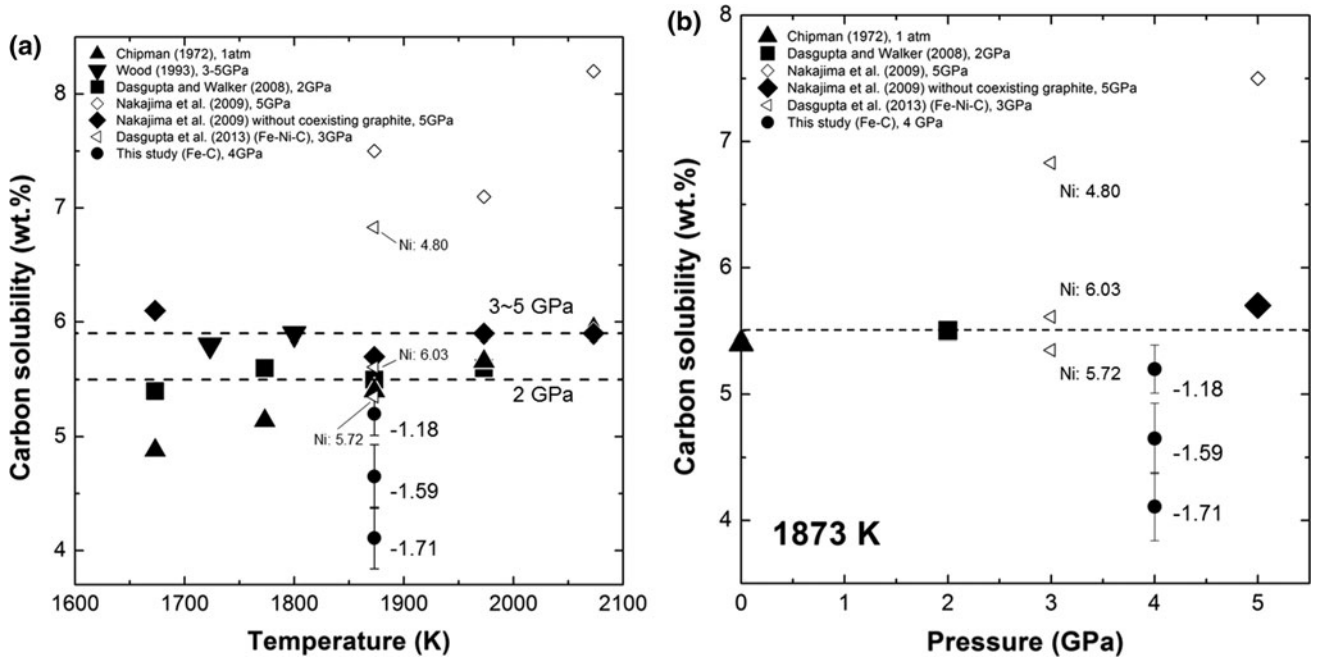


**Fig. 5** Comparison of the C solubility in liquid Fe as a function of **a** temperature and **b** pressure. *Solid triangles*, *inverted triangles,* and *squares* show the results at 1 atm by Chipman (1972), at 3–5 GPa by Wood (1993) and at 2 GPa by Dasgupta and Walker (2008), respectively. *Open diamonds* show the C solubility at 5 GPa reported by Nakajima et al. (2009). *Solid diamonds* show the results of Nakajima et al. (2009) without coexisting graphite crystals. Sideways *open triangles* show the results of the Fe–Ni–C system at 3 GPa by Dasgupta et al. (2013), and we denote the Ni contents in their measurements. *Solid circles* show the present C solubility in liquid Fe composed of Fe–C. The *numbers* represent the oxygen fugacity conditions (ΔIW) of this study. **a** *Dashed lines* show the guides for Dasgupta and Walker (2008) (2 GPa), and Wood (1993) and Nakajima et al. (2009) without coexisting graphite crystals (3–5 GPa). The C solubility in these studies has very weak temperature dependence. **b** The amounts of C at various pressures and at 1,873 K from the present and previous works are plotted. The C solubility may have weak pressure dependence, but it has strong dependence on both oxygen fugacity and Ni content

needed to clarify the processes in the deeper parts of planetary interiors.

## Implications for carbon in the Earth's core and heterogeneity of the Earth's mantle

The present experiments clearly documented that solubility of C in liquid Fe depends on the oxygen fugacity, that is, carbon can dissolve only under oxidizing conditions and carbon does not enter into the core if the oxygen fugacity is as low as around six log units less than the IW buffer. Furthermore, the amount of C is greatly affected by the Si content in liquid Fe, that is, carbon and silicon are mutually exclusive in liquid iron, as shown in Fig. 4a. The metallic phases coexist with olivine and pyroxene and are oversaturated in silica in the Earth's mantle, whereas metallic melts coexist with olivine and periclase, which shows undersaturation in silica in our experiments. The difference in silica activity in silicate could potentially affect the solubility of Si in liquid Fe. Therefore, the solubility of Si in liquid Fe could be higher, and the C content could be lower in the real Earth's mantle and in core-separation processes compared with the present experiments under the same $fO_2$ conditions. Because the solubility of C in liquid Fe has very weak pressure and temperature dependencies, as shown in Fig. 5a, b, the present results could be applied to wide pressure and temperature ranges in various planetary cores. The mutually exclusive nature of carbon and silicon may be important for considering the light elements of the core. Further experiments at pressures relevant to the Earth's core are required.

In the Earth's interior, SiC grains have been reported in some ophiolites and the coexistence of Si and Fe–Si alloy has been reported as inclusions in SiC grains (Trumbull et al., 2009). The $fO_2$ range in the Earth's upper mantle is considered to be about 4 log units above the IW buffer (Frost and McCammon 2008). Under these $fO_2$ conditions, carbon can be stored as graphite/diamond, as carbide or dissolved into metallic iron, as discussed by Dasgupta and Hirschmann (2010). Furthermore, the Si–$SiO_2$ buffer is about 10 log units below the IW buffer at 20 GPa and 1,873 K (Malavergne et al. 2004). Therefore, the upper mantle is too oxidizing to form Si and SiC. Trumbull et al. (2009) proposed a localized highly reducing environment, created by the release of $H_2$ during serpentinization (Dick 1974) or by local and transient reducing conditions

resulting from production of H when diamond grows from a methane-dominated fluid, producing outcomes such as the reduction of FeO-bearing silicates, to form metallic iron. Although the amount of carbon in the Earth differs from that in this study, the coexistence of SiC and Fe–Si as inclusions in SiC grains (Trumbull et al. 2009) is consistent with the present results under the most reducing conditions. The value of $fO_2$ in the present results was about 6.2 log units below the IW buffer, which is enough of a reducing condition to form SiC grains. Although there are no previous data on the difference between the IW buffer and the Si–$SiO_2$ buffer at 4 GPa, it is assumed that the Si–$SiO_2$ buffer is lower than around $\Delta IW = -6.2$ because Si metal is needed to form SiC. The existence of SiC in the Earth's mantle indicates heterogeneity in $fO_2$ and highly localized reducing environments with $\Delta IW < -6.2$.

**Acknowledgments** We thank S. Kamada, K. Nishida, T. Sakai, M. Miyahara, A. Suzuki, and M. Murakami for useful suggestions and discussions. We also thank Prof. Masanori Matsui for the editorial handling and anonymous reviewers for their constructive comments. The in situ X-ray diffraction experiments were performed with the approval of the Japan Synchrotron Radiation Research Institute (JASRI) (Proposal No. 2010A1530 and 2011A1546). This work was supported by a Grant-in-Aid for Scientific Research from the Ministry of Education, Culture, Science, Sport, and Technology of Japan (No. 18104009 and 22000002) to E. Ohtani. This work was conducted as part of the Global COE Program at Tohoku University, "Global Education and Research Center for Earth and Planetary Dynamics".

## References

Anders E, Grevesse N (1989) Abundances of the elements: meteoritic and solar. Geochim Cosmochim Acta 53:197–214

Chipman J (1972) Thermodynamics and phase diagram of the Fe–C system. Metall Mater Trans B 3:55–64

Chipman J, Fulton JC, Gokcen N, Caskey GR (1954) Activity of silicon in liquid Fe–Si and Fe–C–Si alloys. Acta Metall 2:439–450

Corgne A, Keshav S, Wood BJ, McDonough WF, Fei YW (2008a) Metal–silicate partitioning and constraints on core composition and oxygen fugacity during Earth accretion. Geochim Cosmochim Acta 72:574–589

Corgne A, Wood BJ, Fei Y (2008b) C- and S-rich molten alloy immiscibility and core formation of planetesimals. Geochim Cosmochim Acta 72:2409–2416

Dasgupta R, Hirschmann MM (2010) The deep carbon cycle and melting in Earth's interior. Earth Planet Sci Lett 298:1–13

Dasgupta R, Walker D (2008) Carbon solubility in core melts in a shallow magma ocean environment and distribution of carbon between the Earth's core and the mantle. Geochim Cosmochim Acta 72:4627–4641

Dasgupta R, Hirschmann MM, Withers AC (2004) Deep global cycling of carbon constrained by the solidus of anhydrous, carbonated eclogite under upper mantle conditions. Earth Planet Sci Lett 227:73–85

Dasgupta R, Buono A, Whelan G, Walker D (2009) High-pressure melting relations in Fe–C–S systems: Implications for formation, evolution, and structure of metallic cores in planetary bodies. Geochim Cosmochim Acta 73:6678–6691

Dasgupta R, Chi H, Shimizu N, Buono AS, Walker D (2013) Carbon solution and partitioning between metallic and silicate melts in a shallow magma ocean: implications for the origin and distribution of terrestrial carbon. Geochim Cosmochim Acta 102: 191–212

Dick HJB (1974) Terrestrial nickel iron from the Josephine Peridotite, its geologic occurrence, associations, and origin. Phys Earth Planet Inter 24:291–298

Fei Y, Mao H, Mysen BO (1991) Experimental determination of element partitioning and calculation of phase relations in the MgO–FeO–$SiO_2$ system at high pressure and high temperature. J Geophys Res 96:2157–2169

Frost DJ, McCammon CA (2008) The redox state of Earth's mantle. Ann Rev Earth Planet Sci 36:389–420

Frost DJ, Liebske C, Langenhorst F, McCammon CA, Tronnes RG, Rubie DC (2004) Experimental evidence for the existence of iron-rich metal in the Earth's lower mantle. Nature 428: 409–412

Frost DJ, Asahara Y, Rubie DC, Miyajima N, Dubrovinsky LS, Holzapfel C, Ohtani E, Miyahara M, Sakai T (2010) Partitioning of oxygen between the Earth's mantle and core. J Geophys Res 115:B02202

Gessmann CK, Wood BJ, Rubie DC, Kilburn MR (2001) Solubility of silicon in liquid metal at high pressure: implications for the composition of the Earth's core. Earth Planet Sci Lett 184:367–376

Hayashi H, Ohtani E, Terasaki H, Ito Y (2009) The partitioning of Pt–Re–Os between solid and liquid metal in the Fe–Ni–S system at high pressure: implications for inner core fractionation. Geochim Cosmochim Acta 73:4836–4842

Isshiki M, Irifune T, Hirose K, Ono S, Ohishi Y, Watanuki T, Nishibori E, Takata M, Sakata M (2004) Stability of magnesite and its high-pressure form in the lowermost mantle. Nature 427:60–63

Keil K (1968) Mineralogical and chemical relationships among enstatite chondrites. J Geophys Res 73:6945–6976

Kerrick DM, Connolly JAD (2001) Metamorphic devolatilization of subducted oceanic metabasalts: implications for seismicity, arc magmatism and volatile recycling. Earth Planet Sci Lett 189:19–29

Kiseeva ES, Yaxley GM, Hermann J, Litasov KD, Rosenthal A, Kamenetsky VS (2012) An experimental study of carbonated eclogite at 3.5–5.5 GPa: implications for silicate and carbonate metasomatism in the cratonic mantle. J Petrol 53:727–759

Lagrange AM, Gratadour D, Chauvin G, Fusco T, Ehrenreich D, Mouillet D, Rousset G, Rouan D, Allard F, Gendron É, Charton J, Mugnier L, Rabou P, Montri J, Lacombe F (2009) A probable giant planet imaged in the β Pictoris disk VLT/NaCo deep L′-band imaging. Astron Astrophys 493:L21–L25

Lord OT, Walter MJ, Dasgupta R, Walker D, Clark SM (2009) Melting in the Fe–C system to 70 GPa. Earth Planet Sci Lett 284:157–167

Ma Z (2001) Thermodynamic description for concentrated metallic solutions using interaction parameters. Metall Mater Trans B 32:87–103

Malavergne V, Siebert J, Guyot F, Gautron L, Combes R, Hammouda T, Borenstajn S, Frost DJ, Martinez I (2004) Si in the core? New high-pressure and high-temperature experimental data. Geochim Cosmochim Acta 68:4201–4211

Mann U, Frost DJ, Rubie DC (2009) Evidence for high-pressure core–mantle differentiation from the metal–silicate partitioning of lithophile and weakly-siderophile elements. Geochim Cosmochim Acta 73:7360–7386

Molina JF, Poli S (2000) Carbonate stability and fluid composition in subducted oceanic crust: an experimental study on $H_2O$–$CO_2$-bearing basalts. Earth Planet Sci Lett 176:295–310

Nakajima Y, Takahashi E, Suzuki T, Funakoshi K (2009) "Carbon in the core" revisited. Phys Earth Planet Inter 174:202–211

Ohtani M (1955) On the activities of Si and C in molten Fe–Si–C alloys. The 70th Report of the Research Institute of Mineral Dressing and Metallurgy, pp 487–501

Roberge A, Feldman PD, Weinberger AJ, Deleuil M, Bouret JC (2006) Stabilization of the disk around β Pictoris by extremely carbon-rich gas. Nature 441:724–726

Seager S, Kuchner M, Hier-Majumder CA, Militzer B (2007) Mass–radius relationships for solid exoplanets. Astrophys J 669:1279–1297

Siebert J, Guyot F, Malavergne V (2005) Diamond formation in metal–carbonate interactions. Earth Planet Sci Lett 229:205–216

Siebert J, Corgne A, Ryerson FJ (2011) Systematics of metal–silicate partitioning for many siderophile elements applied to Earth's core formation. Geochim Cosmochim Acta 75:1451–1489

Trumbull RB, Yang J, Robinson PT, Di Pierro S, Vennemann T, Wiedenbeck M (2009) The carbon isotope composition of natural SiC (moissanite) from the Earth's mantle: new discoveries from ophiolites. Lithos 113:612–620

Urakawa S, Morishima M, Kato T, Suzuki A, Shimomura O (1993) Equation of state for h–BN. Photon Factory Activity Report G 275:383

Van Vechten JA (1973) Quantum dielectric theory of electronegativity in covalent systems. III. Pressure–temperature phase diagrams, heats of mixing, and distribution coefficients. Phys Rev B 7:1479–1507

Wade J, Wood BJ, Tuff J (2012) Metal–silicate partitioning of Mo and W at high pressures and temperatures: evidence for late accretion of sulphur to the Earth. Geochim Cosmochim Acta 85:58–74

Wagner C (1952) Thermodynamics of Alloys. Addison-Wesley Press, Reading, Ma

Wood BJ (1993) Carbon in the core. Earth Planet Sci Lett 117:593–607

Wood JA, Hashimoto A (1993) Mineral equilibrium in fractionated nebular systems. Geochim Cosmochim Acta 57:2377–2388

Wood IG, David WIF, Hull S, Price GD (1996) A high-pressure study of ε-FeSi, between 0 and 8.5 GPa, by time-of-flight neutron powder diffraction. J Appl Crystallography 29:215–218

Zolensky M, Herrin J, Mikouchi T, Ohsumi K, Friedrich J, Steele A, Rumble D, Fries M, Sandford S, Milam S, Hagiya K, Takeda H, Satake W, Kurihara T, Colbert M, Hanna R, Maisano J, Ketcham R, Goodrich C, Le L, Robinson GA, Martinez J, Ross K, Jenniskens P, Shaddad MH (2010) Mineralogy and petrography of the Almahata Sitta ureilite. Meteorit Planet Sci 45:1618–1637